



Cite this: *Nanoscale*, 2015, **7**, 8405

{331}-Faceted trisoctahedral gold nanocrystals: synthesis, superior electrocatalytic performance and highly efficient SERS activity†

Yahui Song,^a Tingting Miao,^a Peina Zhang,^a Cuixia Bi,^a Haibing Xia,*^a Dayang Wang^b and Xutang Tao^a

We investigate the effect of gold (Au) seeds prepared in cetyltrimethylammonium chloride solution (CTAC-Au seeds) on the index facets of trisoctahedral gold nanocrystals (TOH Au NCs). We demonstrate that monodisperse {331}-faceted TOH Au NCs with controllable sizes (from 60 to 255 nm) can be successfully prepared in high yield by using 3.0 nm CTAC-Au seeds or as-prepared 70 nm TOH Au NCs as seeds. We find that the electrocatalytic performance on methanol oxidation and surface enhancement Raman spectroscopy (SERS) activity of {331}-faceted TOH Au NCs is size-dependent. In comparison with well-known nanoporous gold (0.088 mA cm^{-2}), {331}-faceted TOH Au NCs with sizes of 110 nm exhibit fairly high catalytic activity (0.178 mA cm^{-2}) on methanol oxidation (1.0 M) in alkaline media due to the presence of increasing density of atomic steps, ledges, and kinks on the NC surfaces. Their current density is reduced by less than 7% after 500 cycling tests. {331}-Faceted TOH Au NCs with sizes of 175 nm exhibit the highest SERS activity for 4-aminothiophenol (4-ATP) molecules. The enhancement factors of a_1 modes of 4-ATP molecules can reach the order of 10^9 when the 4-ATP concentration is $3 \times 10^{-6} \text{ M}$. Moreover, Raman signals (a_g modes) of 4,4'-dimercaptoazobenzene (DMAB) molecules on TOH Au NCs are stronger than those on spherical Au NCs of comparable size due to the enhanced laser-induced transformation of 4-ATP molecules by high-index {331}-facets during SERS measurement. Furthermore, the SERS intensities of 4-methylbenzenethiol (4-MTP) molecules on TOH Au NCs are also higher than those on spherical Au NCs of comparable size due to sharp extremities.

Received 13th February 2015,
Accepted 1st April 2015

DOI: 10.1039/c5nr01049g
www.rsc.org/nanoscale

1. Introduction

Exquisite control over the shapes, sizes and compositions of metallic nanocrystals (NCs) has been an important and exciting area in the field of colloidal synthesis due to their peculiar

morphology-dependent physical-chemical properties (such as electronic, optical, catalytic, etc.).^{1–5} In catalysis applications, it was found that noble metal NCs with high-index planes generally exhibit much higher catalytic activity than those with the most common stable planes, such as {111}, {100}, and even {110}, because the high-index planes have a large density of atomic steps, ledges, and kinks, which usually serve as active sites for breaking chemical bonds.^{1,6–12} In addition, the sharp corners and edges from high-index faceted metallic NCs can also result in significant electromagnetic field enhancements,¹³ which are rather important in the applications such as surface enhancement Raman spectroscopy (SERS). Thus, controlled synthesis of metal NCs bounded by high-index facets can provide a powerful way for enhancing the catalytic activities of metal NCs^{8,9} as a new generation of catalysts and improving SERS activity.^{13–17}

Trisoctahedron (TOH), a type of high-indexed polyhedron, is bounded by 24 high-index facets with Miller indices of $\{hkl\}$ ($h > l$). Recently, TOH gold (Au) NCs with {221} facets have been successfully synthesized.^{18,19} However, it is still a challenge to synthesize TOH Au NCs enclosed by higher

^aState Key Laboratory of Crystal Materials, Shandong University, Jinan, 250100, P. R. China. E-mail: hbxia@sdu.edu.cn

^bIan Wark Research Institute, University of South Australia, Adelaide, SA 5095, Australia

† Electronic supplementary information (ESI) available: Extra TEM images and extinction spectra of the corresponding TOH Au NCs obtained with CTAB-Au seeds and CTAC-Au seeds, cyclic voltammograms of the corresponding TOH Au NCs with {221} facets and {331} facets in 0.50 M H₂SO₄ medium, cyclic voltammograms of TOH Au NCs with different sizes in 0.50 M H₂SO₄ medium and in 0.50 M KOH medium, the variation of oxidation peak current density of the GCEs modified by the 110 nm TOH Au NCs at different scanning cycle numbers, experimental extinction spectra of TOH Au NCs of different sizes, SERS spectra of 4-ATP molecules on the aggregates of 175 nm TOH Au NCs and 170 nm spherical Au NCs, the normal Raman spectrum of the neat film of the 4-ATP molecule, and summarized data of the Raman intensity and SERS enhancement factors of the TOH Au NCs with different sizes in specific Raman bands. See DOI: 10.1039/c5nr01049g

high-index facets ($h > 2$) because it is difficult to maintain the high-index facets and concave polyhedral shape with high surface energy when the sizes of NCs are in nanoscale. To date, the seed-mediated growth method is still the proverbial workhorse for the synthesis of metal NCs with different sizes.^{19–23} In this method, it is believed that the seeds with sizes smaller than 3 nm have an important effect on the formation of anisotropic nanoparticles (NPs).

Currently, although the growth solution for the synthesis of {221}-faceted TOH Au NCs is composed of cetyltrimethylammonium chloride (CTAC) molecules, the seeds used for the synthesis of TOH Au NCs are still prepared in cetyltrimethylammonium bromide (CTAB) solution. More recently, it also has been noted that because the oxidative etching power of CTAB is weaker than that of CTAC, CTAC works much better than CTAB as a capping agent in both the syntheses of Au seeds and Au@Ag core–shell nanocubes.^{24,25}

Herein, firstly, we investigated how the nature of surfactants, CTAC and CTAB, affects the sizes and shapes of Au seeds. Secondly, we studied how the morphological differences between CTAB-Au seeds and CTAC-Au seeds affect the size, quality and crystal face index of TOH Au NCs. Here we successfully produced {331}-faceted TOH Au NCs with controllable sizes (from 60 to 255 nm) in high yield by using 3.0 nm CTAC-Au seeds or as-prepared 7.0 nm TOH Au NCs as seeds. Lastly, we studied the electrocatalytic performance on methanol oxidation and SERS activity of {331}-faceted TOH Au NCs of different sizes, which appeared superior in comparison with low-index-faceted Au NCs.

2. Experimental section

2.1 Materials

Cetyltrimethylammonium chloride (CTAC, 99%, catalog no. 30232128), cetyltrimethylammonium bromide (CTAB, 99%, catalog no. 30037416), hydrogen tetrachloroaurate tetrahydrate (HAuCl₄·4H₂O, 99%, catalog no. 10010711), sodium borohydride (NaBH₄, 99%, catalog no. 80115862), and L-ascorbic acid (AA, 99%, catalog no. 10004014) were purchased from Sinopharm Chemical Reagent Co., Ltd. 4-Aminothiophenol (4-ATP, 97%, catalog no. 1193028), 4-methylbenzenethiol (4-MTP, 98%, catalog no. 106456) were purchased from Alfa Aesar, and glutathione (GSH, 99%, catalog no. 1090334) from Aladdin. Milli-Q water with a resistance of 18 MΩ cm was used for all experiments. Glassware was thoroughly cleaned with aqua regia and washed with water. *Caution: aqua regia solutions are dangerous and should be used with extreme care; never store these solutions in closed containers.*

2.2 Preparation of CTAB-Au seeds and CTAC-Au seeds

Typically, the preparation of CTAB-Au seeds is as follows. 0.125 mL of an aqueous HAuCl₄ solution (10 mM) and 5 mL of CTAB solution (0.1 M) were added into a 10 mL glass vial at room temperature. Next, 0.30 mL of a freshly prepared ice-cold NaBH₄ solution (10 mM) was injected quickly into the

CTAB-HAuCl₄ solution under vigorous stirring. The mixed solution was stirred for at least 2 min for the complete decomposition of excess NaBH₄. The CTAB-Au seeds were used within 2–5 h after the preparation.

The CTAC-Au seeds were prepared by the same procedure except for the use of CTAC instead of CTAB as the capping agent.

2.3 Synthesis of TOH Au NCs with sizes of 60 to 110 nm via using CTAC-Au seeds

Typically, the preparation of a growth solution is as follows. 5.0 mL of the aqueous solution of CTAC (50 mM), 0.25 mL of the aqueous solution of HAuCl₄ (10 mM) and 50 μL of the aqueous solution of AA (0.1 M) were sequentially added into a 10 mL glass vial under stirring at room temperature to form the growth solution. 0.25 μL of CTAC-Au seed solution was added to the growth solution and mixed thoroughly. The resulting mixture was placed in a water bath for aging at 28 °C. After aging for 12 h, the resulting TOH Au NCs with sizes of 60 nm along the longest axis were separated from the reaction mixture with the aid of centrifugation (10 000 rcf × 8 min). These NCs were redispersed into water and centrifuged two more times to remove the excess reactants. The average sizes of as-prepared TOH Au NCs were increased from 60 to 70, 90 and 110 nm when the volumes of the seed solutions were decreased from 0.25 to 0.125, 0.075 and 0.05 μL. Note: In practical operation, the solution of CTAC-Au seeds was diluted 100 or 1000 times for use while keeping the same amount of seeds.

2.4 Synthesis of TOH Au NCs with sizes of 140 to 255 nm via using as-prepared 70 nm TOH Au NCs as seeds

The procedure for preparing CTAC-TOH Au NCs with a size range from 140 to 255 nm is the same as that of CTAC-TOH Au NCs with a size range from 60 to 110 nm except that the CTAC-Au seeds were replaced by 70 nm TOH Au NCs. Before using, the solution of as-prepared 70 nm TOH Au NCs was concentrated 20 times. When 50 μL of the concentrated solution of 70 nm TOH Au NCs was used, the resulting TOH Au NCs with sizes of 140 nm along the longest axis were separated from the reaction mixture with the aid of centrifugation (8000 rcf × 6 min). These NCs were redispersed into water and centrifuged two more times to remove the excess reactants. The average sizes of as-prepared TOH Au NCs were increased from 140 to 160, 175, 195 and 255 nm when the volumes of 70 nm TOH Au NC solution were decreased from 50 to 40, 30, 20 and 10 μL, respectively.

2.5 Material characterization

Transmission electron microscopy (TEM) images were obtained with JEOL JEM 2100F TEM at an acceleration voltage of 200 kV. A total of 200 particles from TEM images were counted to calculate the average size of TOH Au NCs of each size. In addition, production yield in the present work was defined as the yield of TOH Au NCs *vs.* byproducts (such as spherical and other irregular shapes). UV-vis spectroscopy was

implemented with a Cary 50 spectrophotometer using a 10 mm path length quartz cuvette at room temperature.

2.6 Electrochemical measurements

All electrochemical measurements were performed in a standard three-electrode cell with a CHI660D electrochemical workstation at room temperature. A Pt wire and a Ag/AgCl electrode were used as the counter and reference electrodes, respectively. A glassy carbon electrode (diameter = 3.0 mm) was used as a working electrode and carefully polished and washed before each experiment.

After as-prepared TOH Au NCs were carefully purified from the reaction residuals *via* washing with water with the aid of centrifugation, their aqueous suspensions were dispensed onto the surfaces of the glassy carbon electrodes (GCEs) and dried at room temperature. The deposited NC layer was then coated with 10 μ L of 1 wt% Nafion solution and dried in air at room temperature.

An aqueous solution of H_2SO_4 (0.50 M) was employed as the electrolyte solution for their cyclic voltammograms (CVs). In addition, as-prepared TOH Au NCs were utilized for electrochemical catalysis of methanol oxidation and their CVs were also recorded in 0.50 M KOH containing methanol of different concentrations (in the range of 0 to 3 M). All the solutions were purged with high purity nitrogen (99.99%) for 30 min prior to the tests.

2.7 SERS measurements

Raman spectra were recorded at room temperature using a LabRAM HR 800 spectrograph with 633 nm as an excitation wavelength and 10 s of the acquisition time used for one spectrum. 4-Aminothiophenol (4-ATP) was chosen as a Raman probe for the quantification of SERS enhancements because it can form uniform self-assembled monolayers (SAMs) on Au surfaces with a known packing density.²⁶ In a typical procedure, glass substrates were cleaned in aqua regia for 20 min and then immersed in piranha solution (sulphuric acid/ H_2O_2 = 7 : 3) for another 20 min. The glass substrates were then thoroughly rinsed with water, and dried with N_2 gas. 20 μ L of the aqueous suspensions of Au NCs were dispensed onto the carefully cleaned glass substrates and dried at room temperature. Samples for SERS experiments were prepared by immersing the glass substrates containing TOH Au NCs into a 5 mL ethanol solution of 4-ATP for 1 h. The concentrations of 4-ATP used in our work were in the range of 3×10^{-2} – 3×10^{-7} M. The samples were then taken out and thoroughly rinsed with ethanol and dried with N_2 gas. All samples were used immediately for SERS measurements after preparation. 4-Methylbenzenethiol (4-MTP) molecules were chosen as Raman probes to investigate the effect of the sharp extremities on SERS activity.

The enhancement factors (EFs) of Raman signals were also estimated according to the method reported in the literature.¹³ Two Raman bands of 4-ATP at 1080 and 1578 cm^{-1} were chosen for the EF calculations. The Raman intensity and SERS

EFs of the TOH Au NCs of different sizes in specific Raman bands were estimated and are summarized in Table S1.[†]

3. Results and discussion

3.1 Preparation of CTAB-Au seeds and CTAC-Au seeds

In the seed-mediated growth method, the first step is the preparation of Au seeds. It has been demonstrated that the shape and size distribution of Au seeds are vital for the preparation of nanostructured Au NPs of high quality by the seed-mediated growth.²⁷ It is also known that oxidative etching has an important effect on the formation of single-crystal Au seeds with high uniformity.²⁸

In general, CTAC-Au seeds have better spherical shape and narrower size distribution than CTAB-Au seeds. This is because the chloride ions in CTAC have a stronger oxidative etching power as compared to the bromide ions in CTAB. In addition, the chloride ions released by the Au precursor ($HAuCl_4$) are not sufficient for oxidative etching.²⁸

To acquire the real images of these as-prepared Au seeds, glutathione (GSH) was used to cap the Au seeds at room temperature and to limit their further growth as these ultra-small particles in the solution would experience Ostwald ripening during the drying process on the TEM grids. TEM images of these GSH-capped Au seeds are shown in Fig. 1. As expected, the CTAB-Au seeds have broader size distribution and their average sizes are 4.0 nm while the CTAC-Au seeds have narrower size distribution and their average sizes are 3.0 nm.

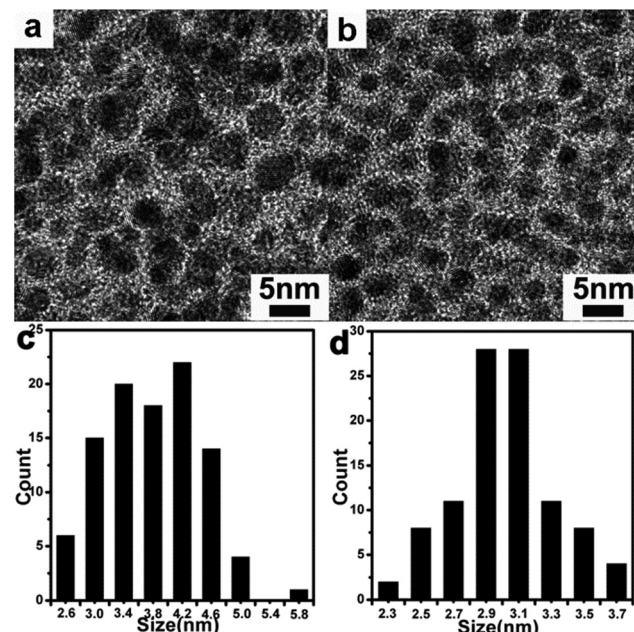


Fig. 1 TEM images (a and b) and histograms (c and d) of CTAB-Au seeds (a and c) and CTAC-Au seeds (b and d). The concentrations of CTAB (or CTAC), $HAuCl_4$, and $NaBH_4$ in the reaction mixture are 92, 0.23, and 0.55 mM, respectively.

Moreover, the shape of CTAC-Au seeds is more spherical than that of the CTAB-Au seeds.

3.2 Synthesis of CTAB-TOH Au NCs and CTAC-TOH Au NCs

3.2.1 Difference in size and quality between CTAB-TOH Au NCs and CTAC-TOH Au NCs. All of the reaction conditions for the preparation of Au seeds are same except that the CTAB is replaced by CTAC. Thus, the same volume of Au seed solution should have the same amount of Au mass. In other words, the smaller the size of the Au seeds, the more Au seeds in the solution. Accordingly, TOH Au NCs of smaller sizes should be obtained when the sizes of Au seeds are smaller as more Au seeds are present in the solution of the same volume.

As is shown in Fig. 2, the average size of CTAC-TOH Au NCs (110 nm) is smaller than that of CTAB-TOH Au NCs (130 nm), which were prepared under the same volume of CTAC-Au seeds and CTAB-Au seeds, respectively. In addition, the quality and production yield of CTAC-TOH Au NCs are relatively better than those of CTAB-TOH Au NCs. Fig. 2c shows the extinction spectra of as-prepared CTAB-TOH Au NCs and CTAC-TOH Au NCs. Obviously, the surface plasmon resonance (SPR) peak position of CTAC-TOH Au NCs is blue-shifted, in comparison with that of CTAB-TOH Au NCs. This result also indicates that the sizes of CTAC-TOH Au NCs are smaller than those of CTAB-TOH Au NCs. The same results were also concluded from TOH Au NCs of other sizes which were prepared by using CTAC-Au seeds and CTAB-Au seeds (Fig. S2 and S3, ESI†). Thus, the size and shape of as-prepared Au seeds indeed have an effect on the synthesis of TOH Au NCs.

3.2.2 Difference in the crystal face index between CTAB-TOH Au NCs and CTAC-TOH Au NCs. Besides the difference mentioned above, the surfactant capped on the surfaces of Au seeds is also different, which may lead to a tiny difference in the crystal facets of as-prepared Au seeds. Accordingly, the difference in their surface structure may result in a difference in the crystal face index of the resulting TOH Au NCs. Therefore, the crystal face index of the CTAB-TOH Au NCs and the CTAC-TOH Au NCs, which were prepared under the same reaction conditions except the seeds, was further investigated.

The Miller indices of the edge-on facets of a TOH NC can be determined through an analysis of the projection

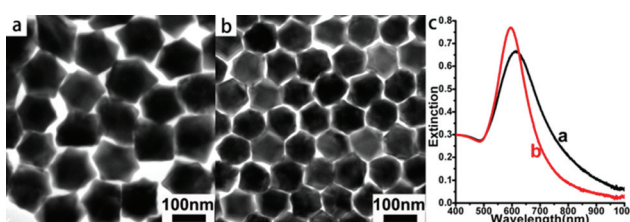


Fig. 2 TEM images (a and b) and extinction spectra (c) of the corresponding TOH Au NCs obtained with CTAB-Au seeds (a, black curve) and CTAC-Au seeds (b, red curve), respectively. The volumes of the Au seed solution used both are 0.05 μ L. The concentrations of CTAC, HAuCl₄, and AA in the reaction mixture are 47, 0.47, and 0.94 mM, respectively.

angles^{29,30} or by the atomic arrangement in the edge-on facets. A geometrical model of a single TOH NC viewed along the <110> direction is shown in Fig. 3a. The values of α , β , and γ corresponding to different Miller indices of a perfect TOH

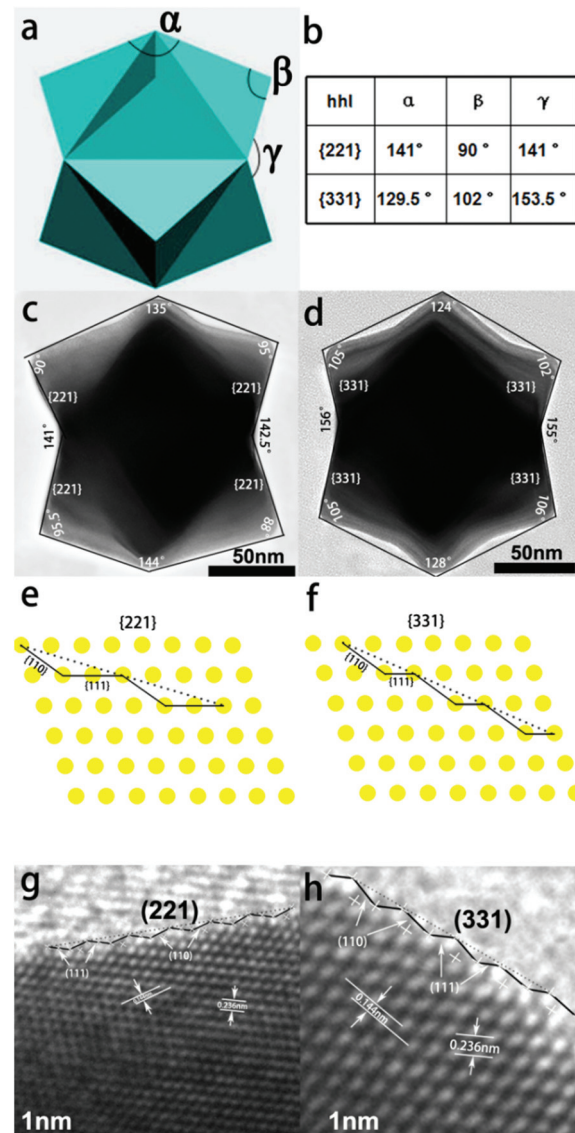


Fig. 3 The geometrical model (a) of a single TOH NC viewed along the <110> direction. A table (b) to summarize the calculated values for the angles of α , β , and γ when the NC is bounded by different crystallographic facets. TEM images (c and d) of the resulting TOH Au NC bounded by {221} (c) and {331} (d) planes, respectively, viewed along the <110> direction. Their sizes along the longest axis are 175 nm and 160 nm, respectively. The measured projection angles are marked. The atomic models (e and f) of the {221} (e) and {331} (f) planes projected from the [110] zone axis. The {221} planes can be visualized as a combination of the (111) terrace of three atomic widths with one (110) step, whereas the {331} planes are made up from the (111) terrace of two atomic widths with one (110) step. HRTEM images (g and h) of edge-on facets viewed along the <110> direction showing the {221} (g) and {331} (h) facets with {111} terraces and {110} steps. The centers of surface atoms are indicated by "x".

crystal are given in the table (Fig. 3b). TEM images of CTAB-TOH Au NCs and CTAC-TOH Au NCs (Fig. 3c and d) were prepared from CTAB-Au seeds and CTAC-Au seeds under the same reaction conditions, respectively. Their sizes along the longest axis are 175 nm and 160 nm, respectively. The projection angles are measured and marked (Fig. 3c and d) accordingly. It is found that the values of α , β , γ angles are consistent with the Miller indices of the {221} and {331} facets, respectively. Thus, the crystal face indices of the resulting TOH Au NCs prepared from different Au seeds are indeed different due to the tiny difference in the crystal facets of as-prepared Au seeds.

The Miller indices of high-index facets can also be identified by the atomic arrangement in the edge-on facets. A step notation was firstly introduced by Somorjai and co-workers to illustrate high-index planes exhibiting ordered terrace-step structures.³¹ A face-centered cubic (fcc) gold facet in the [110] zone can be considered to consist of (111) terraces with m atomic rows and (110) steps, represented as $m(111) \times (110)$. Accordingly, (221) and (331) facets can be described as $3(111) \times (110)$ and $2(111) \times (110)$, respectively.²⁹ The corresponding atomic models of {221} and {331} planes with {111} terraces and {110} steps are shown in Fig. 3e and f, respectively. HRTEM images of edge-on facets of CTAB-TOH Au NCs and CTAC-TOH Au NCs projected along the <110> direction (Fig. 3g and h) further confirm that their edge-on facets are {221} and {331} planes, respectively.

By careful comparison with previous results,^{19,20,32–34} we found that these CTAB-Au seeds and CTAC-Au seeds indeed affected the size, quality and crystal face index of TOH Au NCs. For instance, when the same CTAB-stabilized Au seeds are used, Au NCs with {730} facets^{20,32} and {221} facets¹⁹ are obtained in the growth solution composed of CTAB and CTAC, respectively. When the same growth solutions of CTAC solution are used, Au NCs with {221} facets¹⁹ and {331} facets are obtained by using CTAB-Au seeds and CTAC-Au seeds, respectively. When the same CTAC-stabilized Au seeds and the growth solution of CTAC solution are used, Au NCs with {hk0} facets^{33,34} and {331} facets are obtained with the seed sizes of 7.0 nm and 3.0 nm, respectively.

3.2.3 Difference in electrocatalytic performance between CTAB-TOH Au NCs and CTAC-TOH Au NCs in acidic media. In general, the high-index facets of a single crystal possess a high density of low-coordinated atoms such as steps, edges, and kinks, which can serve as highly active sites for adsorption and catalysis. Moreover, NCs with high-index facets^{15,35–37} are generally more active than those with the low-index facets. Thus, cyclic voltammetry (CV) was used to evidence the difference in the crystal face index of the resulting TOH Au NCs (Fig. S3, ESI†) via the intrinsic differences between the electrochemical behaviors of {221} and {331} facets. In the anodic scans of the CVs of metallic Au in acidic solution, the peak positions in the region 1.00–1.50 V are attributed to the formation of a monolayer of gold oxide. The first peak at 1.20 V corresponds to the first sublattice OH[−] deposition, accompanied by the desorption of specifically adsorbed anions.^{38,39} The second sharp

peak at 1.27 V corresponds to OH[−] adsorption on the second sublattice, thereby completing a full monolayer of OH[−] adsorption on the surfaces of Au NCs.³⁹ Moreover, the replacement of adsorbed anions with OH[−] is relatively easier in {110} facets than {111} facets as the {110} facets are more active than {111} facets. The distinct electrochemical behaviors of the Au NCs bounded with different facets in an acidic solution were also demonstrated in a recent work.⁴⁰ The oxidation peaks of the {111}-bounded Au NCs are located at around 1.15 V and 1.33 V while those of {110}-bounded Au NCs are at about 1.15 V and 1.23 V. Since (221) and (331) facets can be described as $3(111) \times (110)$ and $2(111) \times (110)$, respectively, the proportion of {110} facets in (331) facets of CTAC-TOH Au NCs is higher than that in (221) facets of CTAB-TOH Au NCs. In addition, the replacement of anions with OH[−] in CTAC-TOH Au NCs enclosed by {331} facets is relatively easier than that in CTAB-TOH Au NCs enclosed by {221} facets. It is observed that the relative intensity of the peaks located at 1.23 V to 1.15 V in the CV of CTAC-TOH Au NCs is higher than that in the CV of CTAB-TOH Au NCs although the positions of oxidation peaks of CTAC-TOH Au NCs and CTAB-TOH Au NCs are rather close. Moreover, CTAC-TOH Au NCs show a much higher oxidation peak than CTAB-TOH Au NCs (Fig. S3, ESI†).

3.3 Synthesis of {331}-faceted CTAC-TOH Au NCs of different sizes

3.3.1 Synthesis of {331}-faceted CTAC-TOH Au NCs with a size range from 60 to 110 nm. {331}-Faceted CTAC-TOH Au NCs with a size range from 60 to 110 nm were prepared by using 3.0 nm CTAC-Au seeds. Despite the presence of byproducts such as pentagonal bipyramids, the production yield of {331}-faceted TOH Au NCs is >90% (*versus* other products). As is shown in Fig. 4a–d, the average sizes of {331}-faceted TOH Au NCs along the longest axis can be tuned from 60 to 70, 90 and 110 nm with the decrease of the volume of the Au seed solution from 0.25 to 0.125, 0.075 and 0.05 μ L. However, vertices of CTAC-TOH Au NCs with sizes of 60 nm are still not very sharp. On increasing the size, vertices of CTAC-TOH Au NCs become sharper (Fig. 4a–d). Thus, CTAC-TOH Au NCs with sizes of 70 nm are further used as seeds for the synthesis of TOH Au NCs with bigger sizes. Fig. 4e shows the SPR spectra of as-prepared TOH Au NCs with various average sizes. The TOH Au NCs with sizes of 60 nm still have a symmetric SPR band and no nonzero extinction baseline at longer wavelengths. However, the TOH Au NCs with sizes from 70 to 110 nm exhibit band broadening and remarkable nonzero extinction baseline at longer wavelengths. In addition, the SPR peaks of the NCs obviously red-shift from 552 to 565, 578 and 597 nm and become broader when their sizes increase from 60 to 70, 90 and 110 nm. The SPR band broadening may be ascribed to the sharpness increase of the vertexes of the TOH Au NCs as the NC size increases, or to the excitation of multipolar modes.^{19,41} In addition, as compared to spherical Au NCs of comparable sizes, the sharp extremities of the TOH Au NCs, which can intensify the polarization,^{19,42,43} can also result in the red-shift of the SPR bands.

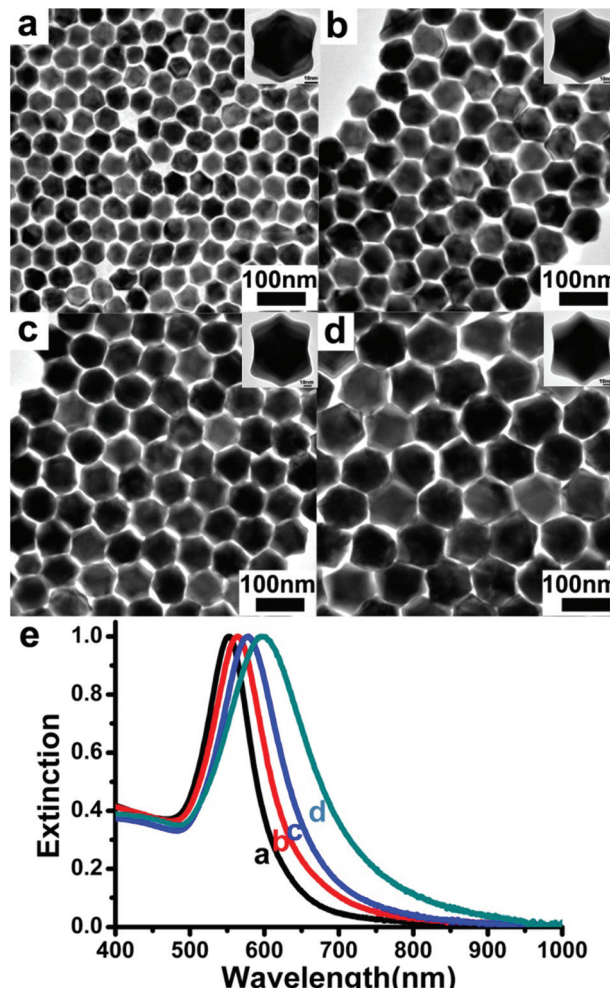


Fig. 4 TEM images (a–d) and extinction spectra (e) of the corresponding TOH Au NCs obtained under different volumes of Au seed solution: 0.25 μ L (a, 60 nm and black curve), 0.125 μ L (b, 70 nm and red curve), 0.075 μ L (c, 90 nm and blue curve), and 0.05 μ L (d, 110 nm and dark cyan curve). The insets (in a–d) are the TEM images of the corresponding TOH Au NC viewed along the <110> direction. The concentrations of CTAC, HAuCl₄, and AA in the growth solution are 47, 0.47, and 0.94 mM, respectively.

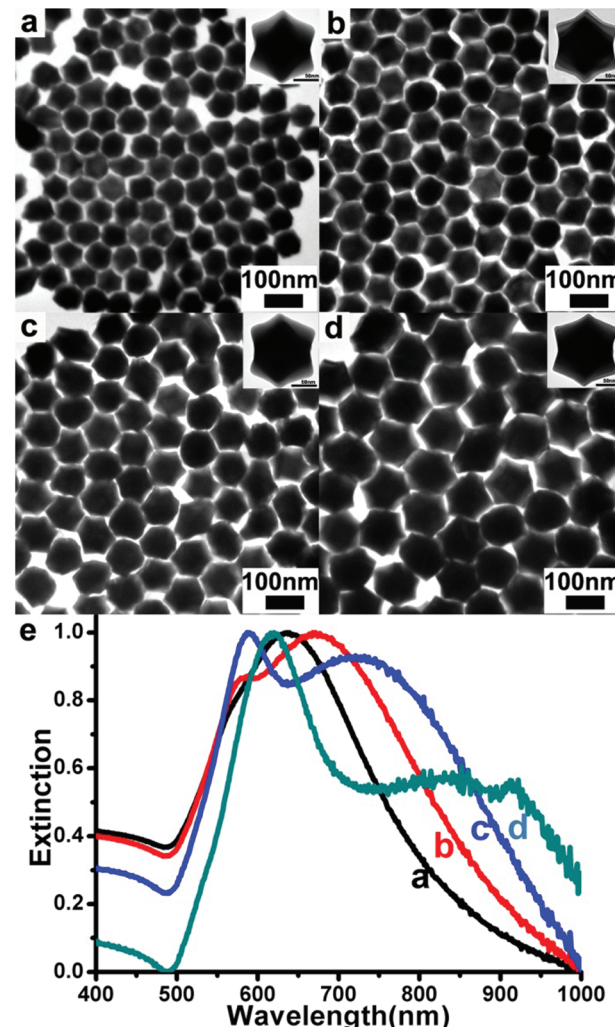


Fig. 5 TEM images (a–d) and extinction spectra (e) of the corresponding TOH Au NCs obtained under different volumes of seed solutions of 70 nm TOH Au NCs: 50 μ L (a, 140 nm and black curve), 30 μ L (b, 175 nm and red curve), 20 μ L (c, 195 nm and blue curve) and 10 μ L (d, 255 nm and dark cyan curve). The insets (in a–d) are the TEM images of the corresponding TOH Au NC viewed along the <110> direction. The concentrations of CTAC, HAuCl₄, and AA in the reaction mixture are 47, 0.47, and 0.94 mM, respectively.

3.3.2 Synthesis of {331}-faceted CTAC-TOH Au NCs with a size range from 140 to 255 nm. For the preparation of TOH Au NCs with larger sizes, the shape uniformity and size distribution become worse by using 3.0 nm CTAC-Au seeds. Thus, newly prepared 70 nm TOH Au NCs were used as seeds for the synthesis of {331}-faceted TOH Au NCs with a size range from 140 to 255 nm (Fig. 5). Similarly, the sizes of the TOH Au NCs can be tuned by varying the amount of the seed solution of TOH Au NCs. As is shown in Fig. 5, the TOH shape of the NCs with a size range from 140, to 175, 195 and 255 nm is well-maintained, and their size distribution still remains narrow despite the increase in the NC dimensions. In addition, the production yields of these Au NCs with a well-defined TOH shape are still higher than 90%. Fig. 5e shows the SPR spectra of as-prepared TOH Au NCs with larger sizes. The TOH Au NCs

obtained with sizes of 140 nm still have a symmetric SPR band, but they also exhibit band broadening and remarkable nonzero extinction baseline at longer wavelengths. When the NC size is bigger than 175 nm, the maximum SPR peak is not a single band, but a shoulder peak starts to appear due to the phase retardation effects⁴⁴ (for 175 nm Au NCs) and develops at lower wavelengths (for 195 nm and 255 nm Au NCs), which is attributed to a quadrupolar resonance while the main (dipolar resonance) band red-shifts and broadens further. For example, Au NCs with a diameter of 195 nm have a dipolar resonance (peaking at 727 nm) and a quadrupolar resonance (peaking at 588 nm) while well defined quadrupolar resonances (peaking at 619 nm) are observed for larger 255 nm NCs.

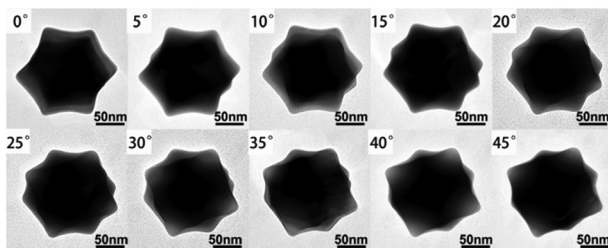


Fig. 6 A set of TEM images of a single TOH Au NC, 175 nm in size, recorded at different tilting angles with x as the axis of rotation from 0° to 45° . The concentrations of CTAC, HAuCl₄, and AA in the reaction mixture are 47, 0.47, and 0.94 mM, respectively.

It seems that not all Au NCs are TOH shaped. A set of TEM images of the same TOH Au NC is recorded at different tilting angles with x as the axis of rotation from 0° to 45° (Fig. 6). It reveals the different trisoctahedral shapes of as-prepared Au NCs under TEM observation. We believe that the different shapes observed on the TEM images are due to the different tilting angles of each single TOH NC on the copper grids.

3.4 Influence of AA concentration on the morphology of Au NCs

TOH shaped Au NCs are kinetic-controlled products. Thus, AA concentration also has an effect on the morphology of Au NCs. For example, the optimal AA concentration for the synthesis of 90 nm TOH Au NCs (Fig. 4b) is 0.94 mM.

When the AA concentration is about 0.56 mM, Au(III) ions cannot be totally reduced, thus leading to the formation of quasi-spherical Au NCs (Fig. 7a). When the AA concentration increases to about 0.71 mM (still lower than optimal AA concentration), Au(III) ions can be totally reduced. However, the reduction rate is still slow, thus leading to a slow growth rate of NC. Accordingly, the morphology of as-prepared Au NCs is not the perfect TOH shape, with its vertices not sharp and just transformed from quasi-spherical to the TOH shape (Fig. 7b). When the AA concentration increases to about 1.88 mM (higher than optimal AA concentration), the reduction rate becomes faster, thus leading to the fast growth rate of the NC and even uneven growth rates on different facets of seeds. Accordingly, some of the Au NCs show imperfect TOH shapes (Fig. 7c). The shape transformation from quasi-spherical to TOH is clearly observed from their TEM images. However, the extinction spectra among imperfect and perfect TOH Au NCs are nearly identical (Fig. 7d).

3.5 Electrochemical characterization of {331}-faceted CTAC-TOH Au NCs of different sizes

It is well known that Au NCs with high-index facets are expected to have a high electrocatalytic performance on methanol oxidation. Here we tested {331}-faceted CTAC-TOH Au NCs of the five sizes obtained and compared their performance in order to select the best catalyst (Fig. S4 and S5, ESI†). Cyclic voltammograms (CVs) of TOH Au NCs with different sizes were

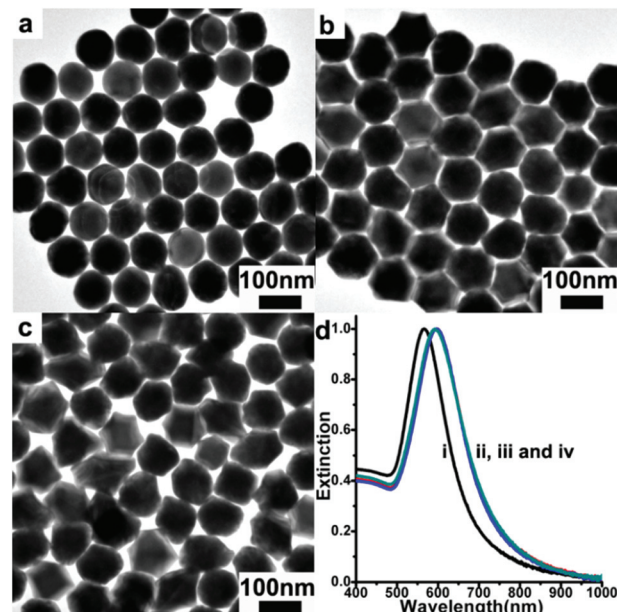


Fig. 7 TEM images (a–c) of the Au NCs prepared in the presence of different AA concentrations: 0.56 mM (a), 0.71 mM (b), and 1.88 mM (c). The extinction spectra (d) of as-prepared Au NCs are normalized by their respective peak intensity: 0.56 mM (i, black curve), 0.71 mM (ii, red curve), and 1.88 mM (iii, dark cyan curve). The extinction spectrum of Au NCs in Fig. 4b prepared in the presence of 0.94 mM AA (iv, blue curve) is also shown for better comparison.

performed in 0.50 M H₂SO₄ medium. The currents are normalized by the Au mass loaded on the electrodes and the scan rates are 50 mV s⁻¹. Although they have different sizes, all CTAC-TOH Au NCs tested are bounded by {331}-facets. Thus, the two oxidation peak potentials in the anodic scan of the CVs are also close, which are 1.198 V and 1.270 V, respectively (Fig. S4, ESI†). In addition, it is found that the areas of reduction peaks of these TOH Au NCs on GCEs are size-dependent; CTAC-TOH Au NCs with sizes of 110 nm bear the maximum area after normalization.

It is known that the adsorption of OH⁻ anion on the Au surface has a promoting role in the electro-oxidation of methanol or other alcohol molecules.^{45,46} Thus, the electrocatalytic performance of CTAC-TOH Au NCs on methanol oxidation was investigated in alkaline media. On the basis of the assumption that the charges associated with the reduction of oxide species are 0.493 mC cm⁻² for Au surfaces, the electrochemically active surface area (ECSA) of the CTAC-TOH Au NCs is theoretically calculated from the observed charges in 0.50 M KOH solution at room temperature at a scan rate of 20 mV s⁻¹ (Fig. S5a, ESI†). The mass normalized ECSA values of TOH Au NCs with sizes of 90, 110, 140, 160, and 195 nm are calculated to be 0.91, 0.86, 0.83, 0.79, and 0.60 m² g⁻¹ (Table S2†), respectively. It is reasonable that the ECSA values decrease with increasing NC size. Fig. S5b† depicts the CVs of the GCEs modified by CTAC-TOH Au NCs of different sizes. The GCE modified by 110 nm CTAC-TOH Au NCs exhibits the highest

electrocatalytic activity ($1.53 \text{ A g}_{\text{Au}}^{-1}$) by displaying the highest mass normalized current density under the same conditions (Fig. S5b and Table S2, ESI†). The currents of these CTAC-TOH Au NCs are also normalized with respect to the ECSA values to obtain their specific activity (Fig. S5c, ESI†). The current density of the 110 nm CTAC-TOH Au NCs still is the largest (0.178 mA cm^{-2}). All these results indicate that the 110 nm CTAC-TOH Au NCs have the best electrocatalytic performance for methanol oxidation (Table S2†). In addition, the current density of the 110 nm TOH Au NCs (0.178 mA cm^{-2}) is about 1.52-fold, 1.73-fold, 2.02-fold and 2.74-fold larger than that of hollow nanoporous Au nanoparticles (0.117 mA cm^{-2})⁴⁷ reported recently, nanoporous gold freestanding films (0.103 mA cm^{-2})⁴⁸ or nanoporous gold (0.088 mA cm^{-2}),⁴⁹ and spherical Au NPs (0.065 mA cm^{-2})⁴⁸ in the positive-going scan, respectively. These results should be attributed to the exposure of their intrinsic active sites (including the high density of atomic steps, ledges, and kinks) to the high-index facets of TOH Au NCs.

Fig. 8a shows the typical CVs of GCEs modified by the 110 nm TOH Au NCs for methanol oxidation of different concentrations in 0.50 M KOH medium. Fig. 8b shows that the calculated current density of GCEs modified by the 110 nm TOH Au NCs linearly increases from 0.10 mA cm^{-2} to 0.40 mA cm^{-2} with methanol concentration increasing from 0.50 M to 3.0 M. The oxidation peak position of GCEs modified by the

110 nm TOH Au NCs with maximum current intensity is around 0.244 V; the higher the methanol concentration, the more negative is the oxidation peak position. Because methanol oxidation is controlled by the adsorption of OH^- anions during the positive potential sweep, the scan rate can strongly influence the methanol oxidation reaction.⁴⁸ Fig. 8c shows the effect of scan rates on the electrochemical oxidation of methanol at GCEs modified by the 110 nm TOH Au NCs in the alkaline solution. As expected, the slower the scan rate, the higher the oxidation current is in the negative potential scan. On the other hand, the slower the scan rate, the smaller is the peak corresponding to the gold oxide reduction in the negative-going potential sweep. When the scan rate is reduced to 10 mV s^{-1} , the reduction current peak almost disappears. Fig. 8d shows a fairly linear relationship between the oxidation peak current density and the scan rate, indicating that the electrode reaction is a surface-controlled process.⁴⁸

Fig. 9 shows the potential-range dependence of the GCEs modified by the 110 nm TOH Au NCs at a sweep rate of 20 mV s^{-1} in 0.50 M KOH medium containing 1.0 M methanol. In the positive-going potential sweep, the large current peaks simultaneously involve the methanol oxidation and gold oxide formation. As the positive potential limit gradually increases, the cathodic peaks corresponding to gold oxide reduction appear at the potential limit of 0.3 V and finally reach the maximum value at the potential limit of 0.5 V. As indicated in these CVs, the gold surface oxide formation can occur at potentials of 0.24 V.

In general, the decrease in the current density is attributed to the decrease of surface active sites of TOH Au NCs with high index facets after the repetitive electrochemical cycles.⁵⁰ Fig. 10 shows that the oxidation peak current density of GCEs modified by 110 nm TOH Au NCs is reduced by less than 7%

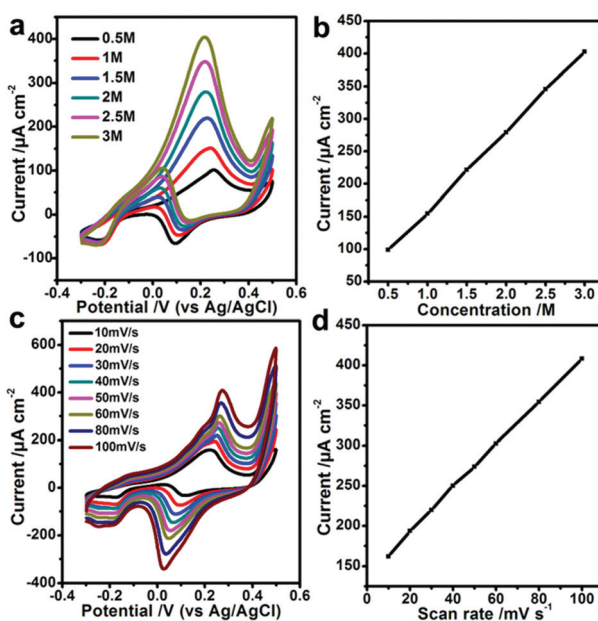


Fig. 8 (a) Cyclic voltammogram (CVs) curves of methanol at different concentrations bearing 0.5 M KOH at the GCEs modified by the 110 nm TOH Au NCs. (b) Plot of calibrated oxidation peak current vs. methanol concentration. The scan rate is 20 mV s^{-1} . (c) CV curves of 1.0 M methanol bearing 0.5 M KOH at the GCEs modified by the 110 nm TOH Au NCs at different scan rates. Scan rates were 100, 80, 60, 50, 40, 30, 20, and 10 mV s^{-1} , respectively. (d) Plot of calibrated oxidation peak current vs. scan rate.

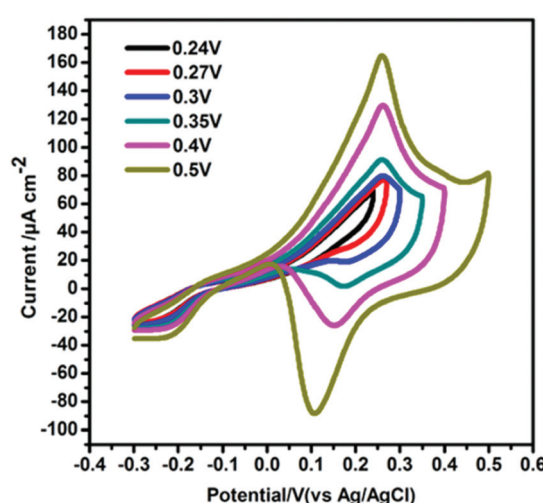


Fig. 9 Cyclic voltammogram (CVs) curves for the electro-oxidation of methanol at the GCEs modified by the 110 nm TOH Au NCs in 0.50 M KOH medium containing 1.0 M methanol with different positive potential limits. The scan rate is 20 mV s^{-1} .

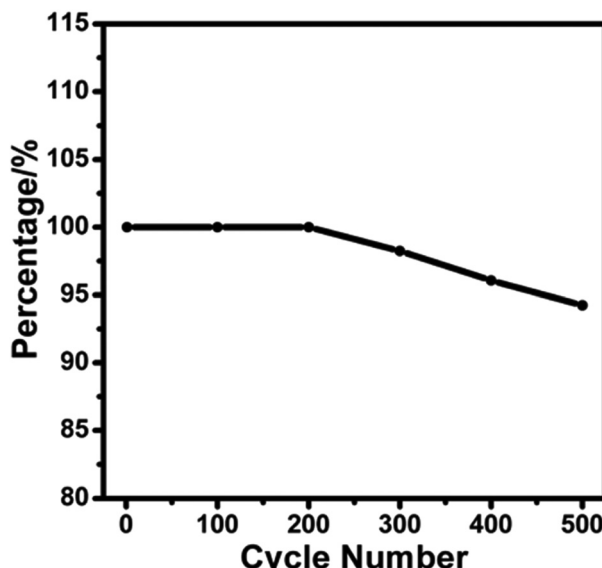


Fig. 10 Plot of the calibrated CV oxidation peak current density vs. the cycling number. The CV curves are recorded in 0.50 M KOH medium containing 1.0 M methanol with GCEs modified by TOH Au NCs with 110 nm in size. The scanning rate is 20 mV s⁻¹.

(Fig. S6, ESI†) while that of pure 12 nm Au NCs is reduced to about 23% after 500 cycles of electrochemical oxidation of methanol.⁴⁸ Interestingly, the oxidation peak intensity is unchanged after 200 cycles. The results unambiguously demonstrate that the TOH Au NCs have superior stability.

3.6 SERS measurements of {331}-faceted CTAC-TOH Au NCs of different sizes

It is known that the electromagnetic fields can be enormously enhanced at the surface vertices and edges upon plasmonic excitation.¹³ Moreover, the electromagnetic field between two or more closely spaced NPs can also be amplified dramatically, thus leading to the observation of enhancement factors (EFs) several orders of magnitude greater than those of the individual NPs.^{51,52} As such, aggregates of TOH-shaped Au NCs with sharp vertices should have highly efficient SERS activity. In addition to the NP geometries, the coupling between SPR bands and the excitation laser is also a key factor that determines SERS enhancements.¹³ The size-dependent SPR bands of as-prepared CTAC-TOH Au NCs (Fig. S7, ESI†) allowed us to fine-tune their SPR bands with respect to the excitation laser wavelength and quantify the SERS enhancements.

Fig. 11a shows the SERS spectra of 4-ATP molecules adsorbed on the aggregates of differently-sized TOH Au NCs. At the excitation laser wavelength of 633 nm, multiple Raman bands between 800 and 1800 cm⁻¹ are strongly enhanced. For instance, two strong Raman bands at 1080 and 1578 cm⁻¹ contribute to the vibration modes of $\nu_{\text{CS}}(\text{a}_1 \text{ mode})$ and $\nu_{\text{CC}}(\text{a}_1 \text{ mode})$ of 4-ATP molecules, respectively.⁵³ In addition, three other apparent Raman bands at 1140, 1391 and 1434 cm⁻¹, are not “ b_2 mode” peaks of 4-ATP molecules, but contributed

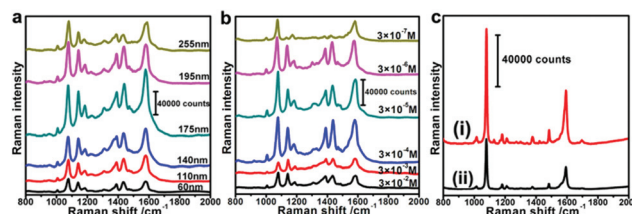


Fig. 11 (a) Representative SERS spectra of 4-ATP molecules (3×10^{-4} M) on the aggregates of CTAC-TOH Au NCs of different sizes on glass substrates. (b) SERS spectra of 175 nm CTAC-TOH Au NCs at different concentrations of the 4-ATP molecule. (c) SERS spectra of 4-MTP molecules (3×10^{-4} M) on the aggregates of 175 nm TOH Au NCs (i) and 170 nm spherical Au NCs (ii), respectively. The excitation laser wavelength for Raman measurements is 633 nm. The acquisition time is 10 s.

by the a_g mode of 4,4'-dimercaptoazobenzene (DMAB) molecules,⁵⁴ which result from the laser-induced transformation of 4-ATP in the presence of {331}-faceted TOH Au NCs during SERS measurement.^{54–56} In contrast, corresponding Raman signals (a_g mode of DMAB molecules) in the SERS spectrum of spherical Au NCs of comparable sizes are rather weak (Fig. S8†), indicating that the formation of DMAB molecules is insignificant in the presence of spherical Au NCs enclosed with low index-facets.⁵⁵ Moreover, SERS activity of as-prepared TOH Au NCs increases and then decreases with their sizes; 175 nm CTAC-TOH Au NCs show the maximum SERS signals.

We also estimated the EFs of 175 nm CTAC-TOH Au NCs on the basis of normal Raman signals obtained from neat 4-ATP films (Fig. S9, ESI†). The EFs of a_1 modes of 4-ATP molecules on the aggregates of 175 nm CTAC-TOH Au NCs were estimated to be of the order of 10^7 (Table S1, ESI†). It is known that the EFs of Raman signals are strongly dependent on the concentration of the probe molecule. Thus, SERS signals of 4-ATP of different concentrations on the aggregates of 175 nm TOH Au NCs were further performed and are shown in Fig. 11b. One can see that all the Raman signals of 4-ATP molecules on the aggregates of 175 nm TOH Au NCs increase and then decrease with the concentration of 4-ATP molecules. Moreover, all the Raman signals obtained are the strongest at a concentration of 3×10^{-4} M. Furthermore, the EFs of a_1 modes of 4-ATP molecules can reach the order of 10^9 when the concentration of 4-ATP molecules is 3×10^{-6} M.

To investigate the effect of the sharp extremities on SERS activity, we also conducted SERS measurements of 4-methylbenzenethiol (4-MTP) on the aggregates of 175 nm TOH Au NCs and spherical Au NCs of comparable sizes (Fig. 11c) to avoid the influence of DMAB molecules. It is worth pointing out that the intensities of Raman signals in the SERS spectra of TOH Au NCs are higher than those of spherical Au NCs of comparable sizes. The pronounced SERS efficiencies can be attributed to the presence of large numbers of sharp extremities, edges, and interparticle gaps in the aggregates of 175 nm TOH Au NCs, which can serve as “hot spots”,^{14,57} thus resulting in enhanced SERS signals. Moreover, the Raman signals at 1140, 1391 and 1434 cm⁻¹ of 4-MTP molecules on the aggre-

gates of TOH Au NCs or spherical Au NCs disappear, indicating that these Raman signals in the spectra of 4-ATP molecules are indeed contributed by the a_g mode of DMAB molecules as 4-MTP molecules cannot transform into DMAB molecules under laser illumination in the presence of {331}-faceted TOH Au NCs or spherical Au NCs during SERS measurement.

4. Conclusions

In summary, we have successfully synthesized monodisperse {331}-faceted TOH Au NCs with sizes ranging from 60 to 255 nm in high yield by using CTAC-Au seeds or as-prepared 70 nm TOH Au NCs as seeds. When the same growth solution is used, {331}-faceted TOH Au NCs are obtained by using CTAC-Au seeds while {221}-faceted ones are obtained by using CTAB-Au seeds. We demonstrate that the electrocatalytic performance of {331}-faceted TOH Au NCs for methanol oxidation and their SERS activity are size-dependent. By comparison with SERS intensities of 4-ATP molecules on {331}-faceted TOH Au NCs and spherical Au NCs of comparable sizes, we find that stronger Raman signals (a_g modes) of DMAB molecules on TOH Au NCs are observed due to the enhanced laser-induced transformation of 4-ATP molecules by high-index {331} facets during SERS measurement. Furthermore, sharp extremities also endow as-prepared TOH Au NCs with an enhanced SERS activity. Therefore, the TOH Au NCs bounded with high-index facets will have promising potential for technical applications in plasmonics, SERS-based detection, and catalysis.

Acknowledgements

This work was financially supported by the Natural Science Foundation of China (51172126, 21473105, 51002086, 51227002 and 51272129) and the Shandong Provincial Natural Science Foundation for Distinguished Young Scientists (JQ201405). H. X. is grateful to the Program for New Century Excellent Talents in University (NCET-10-0553). D. W. thanks the Australian Research Council for financial support (DP120102959).

Notes and references

- 1 F. Ke, B. Solomon, Y. Ding, G. Xiu, S. Sun, Z. Wang and X. Zhou, *Nano Energy*, 2014, **7**, 179–188.
- 2 M. Mulvihill, A. Tao, K. Benjauthrit, J. Arnold and P. Yang, *Angew. Chem., Int. Ed.*, 2008, **47**, 6456–6460.
- 3 R. A. Alvarez-Puebla and L. M. Liz-Marzán, *Chem. Soc. Rev.*, 2012, **41**, 43–51.
- 4 M. Grzelczak, J. Perez-Juste, P. Mulvaney and L. M. Liz-Marzán, *Chem. Soc. Rev.*, 2008, **37**, 1783–1791.
- 5 K. Zhou and Y. Li, *Angew. Chem., Int. Ed.*, 2012, **51**, 602–613.
- 6 G. A. Somorjai and D. W. Blakely, *Nature*, 1975, **258**, 580–583.
- 7 N. Tian, Z. Zhou, S. Sun, Y. Ding and Z. Wang, *Science*, 2007, **316**, 732–735.
- 8 L. Zhang, W. Niu, W. Gao, L. Qi, J. Lai, J. Zhao and G. Xu, *ACS Nano*, 2014, **8**, 5953–5958.
- 9 Y. Xiong, B. Wiley and Y. Xia, *Angew. Chem., Int. Ed.*, 2007, **46**, 7157–7159.
- 10 S. Sun, A. Chen, T. Huang, J. Li and Z. Tian, *J. Electroanal. Chem.*, 1992, **340**, 213–226.
- 11 Z. Zhou, Z. Huang, D. Chen, Q. Wang, N. Tian and S. Sun, *Angew. Chem., Int. Ed.*, 2010, **49**, 411–414.
- 12 L. Zhang, W. Niu and G. Xu, *Nano Today*, 2012, **7**, 586–605.
- 13 Q. Zhang, N. Large and H. Wang, *ACS Appl. Mater. Interfaces*, 2014, **6**, 17255–17267.
- 14 X. Xia, J. Zeng, B. McDearmon, Y. Zheng, Q. Li and Y. Xia, *Angew. Chem., Int. Ed.*, 2011, **50**, 12542–12546.
- 15 J. W. Hong, S. U. Lee, Y. W. Lee and S. W. Han, *J. Am. Chem. Soc.*, 2012, **134**, 4565–4568.
- 16 Q. Zhang and H. Wang, *ACS Catal.*, 2014, **4**, 4027–4033.
- 17 P. Yin, T. You, E. Tan, J. Li, X. Lang, L. Jiang and L. Guo, *J. Phys. Chem. C*, 2011, **115**, 18061–18069.
- 18 Y. Ma, Q. Kuang, Z. Jiang, Z. Xie, R. Huang and L. Zheng, *Angew. Chem., Int. Ed.*, 2008, **47**, 8901–8904.
- 19 Y. Yu, Q. Zhang, X. Lu and J. Y. Lee, *J. Phys. Chem. C*, 2010, **114**, 11119–11126.
- 20 T. Ming, W. Feng, Q. Tang, F. Wang, L. Sun, J. Wang and C. Yan, *J. Am. Chem. Soc.*, 2009, **131**, 16350–16351.
- 21 H. Wu, C. Kuo and M. Huang, *Langmuir*, 2010, **26**, 12307–12313.
- 22 Y. Yu, Q. Zhang, B. Liu and J. Y. Lee, *J. Am. Chem. Soc.*, 2010, **132**, 18258–18265.
- 23 W. Niu, L. Zhang and G. Xu, *Nanoscale*, 2013, **5**, 3172–3181.
- 24 Y. Ma, W. Li, E. C. Cho, Z. Li, T. Yu, J. Zeng, Z. Xie and Y. Xia, *ACS Nano*, 2010, **4**, 6725–6734.
- 25 H. Li, H. Wu, Y. Zhai, X. Xu and Y. Jin, *ACS Catal.*, 2013, **3**, 2045–2051.
- 26 N. Mohri, S. Matsushita, M. Inoue and K. Yoshikawa, *Langmuir*, 1998, **14**, 2343–2347.
- 27 M. Liu and P. Guyot-Sionnest, *J. Phys. Chem. B*, 2005, **109**, 22192–22200.
- 28 W. Li and Y. Xia, *Chem. – Asian. J.*, 2010, **5**, 1312–1316.
- 29 N. Tian, Z. Zhou and S. Sun, *J. Phys. Chem. C*, 2008, **112**, 19801–19817.
- 30 Y. Ding, Y. Gao, Z. Wang, N. Tian, Z. Zhou and S. Sun, *Appl. Phys. Lett.*, 2007, **91**, 121901–121903.
- 31 M. A. Vanhove and G. A. Somorjai, *Surf. Sci.*, 1980, **92**, 489–518.
- 32 L. Zhang and C. Zhang, *Nanoscale*, 2013, **5**, 5794–5800.
- 33 M. L. Personick, M. R. Langille, J. Zhang and C. A. Mirkin, *Nano Lett.*, 2011, **11**, 3394–3398.
- 34 M. R. Langille, M. L. Personick, J. Zhang and C. A. Mirkin, *J. Am. Chem. Soc.*, 2012, **134**, 14542–14554.
- 35 L. Zhang, W. Niu, Z. Li and G. Xu, *Chem. Commun.*, 2011, **47**, 10353–10355.
- 36 F. Wang, C. Li, L. Sun, H. Wu, T. Ming, J. Wang, J. Yu and C. Yan, *J. Am. Chem. Soc.*, 2011, **133**, 1106–1111.

- 37 J. Zhang, M. R. Langille, M. L. Personick, K. Zhang, S. Li and C. A. Mirkin, *J. Am. Chem. Soc.*, 2010, **132**, 14012–14014.
- 38 A. Hamelin, *J. Electroanal. Chem.*, 1996, **407**, 1–11.
- 39 H. Angersteinkozowska, B. E. Conway, A. Hamelin and L. Stoicoviciu, *Electrochim. Acta*, 1986, **31**, 1051–1061.
- 40 J. Wang, J. Gong, Y. Xiong, J. Yang, Y. Gao, Y. Liu, X. Lu and Z. Tang, *Chem. Commun.*, 2011, **47**, 6894–6896.
- 41 S. Link and M. A. El-Sayed, *J. Phys. Chem. B*, 1999, **103**, 8410–8426.
- 42 R. Jin, Y. Cao, C. A. Mirkin, K. L. Kelly, G. C. Schatz and J. Zheng, *Science*, 2001, **294**, 1901–1903.
- 43 K. L. Kelly, E. Coronado, L. Zhao and G. C. Schatz, *J. Phys. Chem. B*, 2003, **107**, 668–677.
- 44 H. Wang and N. J. Halas, *Adv. Mater.*, 2008, **20**, 820–825.
- 45 Z. Borkowska, A. Tymosiak-Zielinska and G. Shul, *Electrochim. Acta*, 2004, **49**, 1209–1220.
- 46 M. Avramov-Ivic, V. Jovanovic, G. Vlajnic and J. Popic, *J. Electroanal. Chem.*, 1997, **423**, 119–124.
- 47 S. Pedireddy, H. Lee, W. Tjiu, I. Phang, H. Tan, S. Chua, C. Troadec and X. Ling, *Nat. Commun.*, 2014, **5**, 4947.
- 48 H. Xia, Y. Ran, H. Li, X. Tao and D. Wang, *J. Mater. Chem. A*, 2013, **1**, 4678–4684.
- 49 J. Zhang, P. Liu, H. Ma and Y. Ding, *J. Phys. Chem. C*, 2007, **111**, 10382–10388.
- 50 L. Chen, T. Fujita, Y. Ding and M. Chen, *Adv. Funct. Mater.*, 2010, **20**, 2279–2285.
- 51 E. C. Le Ru, M. Meyer, E. Blackie and P. G. Etchegoin, *J. Raman Spectrosc.*, 2008, **39**, 1127–1134.
- 52 Z. Wang, S. Pan, T. D. Krauss, H. Du and L. J. Rothberg, *Proc. Natl. Acad. Sci. U. S. A.*, 2003, **100**, 8638–8643.
- 53 M. Osawa, N. Matsuda, K. Yoshii and I. Uchida, *J. Phys. Chem.*, 1994, **98**, 12702–12707.
- 54 Y. Huang, H. Zhu, G. Liu, D. Wu, B. Ren and Z. Tian, *J. Am. Chem. Soc.*, 2010, **132**, 9244–9246.
- 55 X. Lang, T. You, P. Yin, E. Tan, Y. Zhang, Y. Huang, H. Zhu, B. Ren and L. Guo, *Phys. Chem. Chem. Phys.*, 2013, **15**, 19337–19342.
- 56 P. Xu, L. Kang, N. H. Mack, K. S. Schanze, X. Han and H. L. Wang, *Sci. Rep.*, 2013, **3**, 2997.
- 57 L. Zhang, S. Zhong and A. Xu, *Angew. Chem., Int. Ed.*, 2013, **52**, 645–649.